Multi-disciplinary investigation of fluid seepage on an unstable margin: The case of the Central Nile deep-sea fan.

Germain Bayon, L. Loncke, Stéphanie Dupré, Jean-Claude Caprais, Emmanuelle Ducassou, Sébastien Duperron, Joël Etoubleau, Jean-Paul Foucher, Yves Fouquet, Swanne Gontharet, et al.

Marine Geology
June 2009, Volume 261, Issues 1-4, Pages 92-104
http://dx.doi.org/10.1016/j.margeo.2008.10.008

Multi-disciplinary investigation of fluid seepage on an unstable margin: The case of the Central Nile deep sea fan

G. Bayon[a, *], L. Loncke[b], S. Dupré[a, c], J.-C. Caprais[d], E. Ducassou[e], S. Duperron[f], J. Etoubleau[a], J.-P. Foucher[a], Y. Fouquet[a], S. Gontharet[g], G.M. Henderson[h], C. Huguen[i], I. Klaucke[j], J. Mascle[k], S. Migeon[k], K. Olu-Le Roy[d], H. Ondréas[a], C. Pierre[g], M. Sibuet[d], A. Stadnitskaia[l] and J. Woodside[c]

[a] Département Géosciences Marines, IFREMER, Brest, France
[b] UMR 8110, Université de Picardie Jules Verne, Amiens, France
[c] Sedimentology and Marine Geology Department, Vrije Universiteit, Amsterdam, The Netherlands
[d] Département Etude des Ecosystèmes Profonds, IFREMER, Brest, France
[e] UMR 5805 EPOC, Université de Bordeaux 1, France
[f] UMR 7138, Université Pierre et Marie Curie, Paris, France
[g] LOCEAN, Université Pierre et Marie Curie, Paris, France
[h] Department of Earth Sciences, University of Oxford, UK
[i] LEGEM, Université de Perpignan, Perpignan, France
[j] IFM-GEOMAR, Kiel, Germany
[k] Géosciences Azur UMR 6526, Villefranche-sur-mer, France
[l] Royal Netherlands Institute for Sea Research, Texel, The Netherlands

*: Corresponding author : G. Bayon, Tel.: +33 2 98 22 46 30; fax: +33 2 98 22 45 70, email address : Germain.Bayon@ifremer.fr

Abstract:

We report on a multidisciplinary study of cold seeps explored in the Central Nile deep-sea fan of the Egyptian margin. Our approach combines *in situ* seafloor observation, geophysics, sedimentological data, measurement of bottom-water methane anomalies, pore-water and sediment geochemistry, and ^{230}Th/U dating of authigenic carbonates. Two areas were investigated, which correspond to different sedimentary provinces. The lower slope, at ~ 2100 m water depth, indicates deformation of sediments by gravitational processes, exhibiting slope-parallel elongated ridges and seafloor depressions. In contrast, the middle slope, at not, vert, ~ 1650 m water depth, exhibits a series of debris-flow deposits not remobilized by post-depositional gravity processes.

Significant differences exist between fluid-escape structures from the two studied areas. At the lower slope, methane anomalies were detected in bottom-waters above the depressions, whereas the adjacent ridges show a frequent coverage of fractured carbonate pavements associated with chemosynthetic vent communities. Carbonate U/Th age dates (~ 8 kyr BP), pore-water sulphate and solid phase sediment data suggest that seepage activity at those carbonate ridges has decreased over the recent past. In contrast, large (~ 1 km2) carbonate-paved areas were discovered in the middle slope, with U/Th isotope evidence for ongoing carbonate precipitation during the Late Holocene (since ~ 5 kyr BP at least).

Our results suggest that fluid venting is closely related to sediment deformation in the Central Nile margin. It is proposed that slope instability leads to focused fluid flow in the lower slope and exposure of 'fossil' carbonate ridges, whereas pervasive diffuse flow prevails at the unfailed middle slope.

Keywords: Nile; continental margin; cold seep; U-Th; authigenic carbonate

1 – Introduction

Submarine pockmarks are widespread features on continental margins, which are often related to seepage of gas-rich fluids at the seafloor and/or to the presence of gas hydrates in marine sediments (e.g. Hovland and Judd, 1988; Judd and Hovland, 2007). Over recent years, there has been much interest in the study of seafloor pockmarks because they represent potential pathways for important quantities of gas from sediments to the ocean and, perhaps, to the atmosphere (e.g. Vogt et al., 1999; Paull et al., 2002; Ussler et al., 2003; Dimitrov and Woodside, 2003; Hovland et al., 2002, 2005; Gay et al., 2006). In active seepage sites, expulsion of gas-rich fluids commonly supports the development of chemosynthetic communities and the formation of authigenic carbonates, both of which are of interest for the understanding of biogeochemical and microbiological processes related to fluid seeping.

Increasing evidence of vast submarine pockmark fields in areas of destabilised seafloor sediments has questioned the relationship between slope instability and fluid circulation on continental margins (e.g. Hovland et al., 2002; Gay et al., 2004; Lastras et al., 2004; Loncke et al., 2004; Trincardi et al., 2004). Are sediment slides responsible for fluid release on the seafloor or, instead, does fluid circulation within margin sediments favour mass movements? A recent compilation of published dates for major submarine failures occurring in the North Atlantic area has shown that most sediment failures took place during two distinct periods over the last 45,000 years: the Bølling-Ållerød (15 – 13 ka) and the Preboreal (11 – 8 ka), which correlate with peaks of enhanced atmospheric methane concentrations recorded in ice cores (Maslin et al., 2004). It has been speculated that dissociation of gas hydrates in marine sediments, in response to environmental

82 changes, has been instrumental in triggering such sediment failures, possibly releasing
83 significant quantities of methane into the atmosphere (e.g. Paull et al., 2000; Nisbet,
84 2002; Kennett et al., 2002; Mienert et al., 2005). Isotopic records of atmospheric CH_4 in
85 ice cores suggest, however, that marine gas hydrate reservoirs have remained stable
86 during the Late Quaternary (Sowers, 2006). In-depth investigations of selected key
87 regions are now needed, however, to bring further insights on the mechanisms linking
88 slope instabilities, fluid circulation and methane emission on continental margins (e.g.
89 Mienert, 2004).
90
91 Here, we report on a multidisciplinary study of cold seeps and mass movements
92 explored off Egypt (Eastern Mediterranean basin), which brings interesting information
93 on the relationship between fluid seepage and slope instabilities on continental margins.
94 Fluid-related structures are particularly abundant in the central province of the Nile deep-
95 sea fan, between 1500 and 2500 m water depth - an area where sediments are completely
96 destabilised by gravitational processes (Loncke et al., 2002; Loncke et al., 2004).
97 Selected targets of the Nile deep-sea fan were explored during two expeditions (Nautinil
98 2003 - R/V Atalante; Mimes 2004 - R/V Pelagia), funded through the MEDIFLUX
99 project (ESF Euromargins Programme). This work represents a synthesis of *in situ*
100 seafloor observation with the *Nautile* submersible, geophysical (3.5 kHz profiles, deep-
101 tow sidescan sonar seafloor imagery), sedimentological and geochemical data (dissolved
102 sulphate, elemental analyses, ^{230}Th/U carbonate ages), some of which include preliminary
103 results.
104

2 – Geological setting

The Nile deep sea fan is a large sedimentary wedge, which has developed mainly since the Late Miocene in the eastern Mediterranean Sea (e.g. Salem, 1976). The morphology of the Nile deep sea fan results from the complex interplay between pre-Messinian inherited topography, salt-related deformation, and sediment gravity processes. Salt tectonism (e.g. diapirism, gravity spreading and gliding) on the Nile margin is related to the presence of a ductile Messinian salt layer within the sedimentary edifice (Mascle et al., 2000; Gaullier et al., 2000; Loncke et al., 2006). Sediment mass-wasting (e.g. slumping, debris flows) has occurred on the entire Nile fan, in response to various processes, such as salt-tectonism, sediment overloading and fluid circulation. In particular, the Central Nile Province is characterized by a highly destabilised seafloor surface, which shows repeated sediment failures and debris flows (Loncke et al., 2002; Loncke et al., 2004). Loncke et al. (2004) suggested that sediment instability in the Central Nile Province may be related to circulation of gas-rich fluids within sub-surface sediments.

A large number of seafloor structures related to fluid venting were recognised on the Nile margin during recent geophysical surveys (Fig. 1; Bellaiche et al., 2001; Loncke et al., 2002; Loncke et al., 2004). Numerous gas chimneys and associated mud volcanoes and cones were identified in Eastern (e.g. Isis, Amon, Osiris; see Fig. 1) and Western provinces. Many of these structures have been emplaced in areas where Messinian salt layers are absent in the sedimentary cover or have thinned down significantly, thereby allowing deep pre-Messinian fluids to migrate upward along major faults. Other smaller

seafloor structures related to fluid venting were identified on the Nile margin from ship-borne multibeam acoustic images. They correspond to numerous highly-reflective patches, attributed to small pockmarks and/or mounds (Fig. 1; Loncke et al., 2004). Those patches are clustered in two areas (Fig. 1): in the Eastern province, in close proximity to gas chimneys; and in the Central Nile Province, associated with destabilized sediments. In the Central Province, those highly reflective acoustic patches occur mainly at water depths ranging from ~ 500 m down to 2500 m. One important objective of the MEDIFLUX project was to characterise those acoustic patches identified on ship-borne multibeam seafloor maps and to establish their relationship with fluid seepage and slope instability.

3 – Materials and Methods

3.1. Geophysics

An extensive set of geophysical data (3.5 kHz profiles, Simrad EM12-Dual and EM300-Dual multibeam echosounder and seismic data) was acquired during the Nautinil 2003 expedition, as well as during previous Géosciences-Azur cruises (PrismedII 1998, Fanil 2000 and Vanil 2004), which provided bathymetric and acoustic maps for the entire Nile deep sea fan (Loncke et al., 2004). Multibeam EM12- and EM-300 data were combined and processed at a grid size of 50m/pixel, using the Caraïbes software. High-resolution EdgeTech DTS-1 side-scan sonar data were acquired during the Mimes 2004 expedition. The deep tow side scan sonar was deployed and towed at around 100 m above the seafloor and operated at a 75-kHz frequency, with a 1500m wide swath of the seafloor.

151

152 3.2. *Nautile* dives

153 *Nautile* dives took place in two different areas on the Central Nile Province: 1) the lower
154 slope, at ~ 2100 m water depth (dives NL6 and NL14; Fig. 1), and 2) the middle slope, at
155 ~ 1650 m water depth (dive NL7; Fig. 2B,C). Microbathymetric profiles along each dive
156 transect were acquired using *Nautile* sensors (pressure sensor and sounder). A methane
157 sensor (Capsum METS) was installed on the Nautile frame to detect methane in bottom-
158 waters. Note that concentrations measured with the methane sensor are qualitative only.

159

160 3.3. Sediment cores

161 A set of push-cores and blade-cores (i.e. a submersible-mounted corer equipped with a
162 guillotine-like cutter, which allows efficient sampling of unconsolidated sediments) was
163 collected in the Central Nile province during the *Nautile* dives. One piston core (NLK11)
164 was also collected from the lower slope during the Nautinil cruise. The position of all
165 sediment cores used for this study is given in Table 1 and shown in Figs. 1, 3B,C and 4.
166 Push-cores NL14-PC1 and NL14-PC3 were retrieved in carbonate ridge areas (see
167 description of fluid-venting structures in section 4.2). Push-core NL6-PC1 was collected
168 from a small pockmark on the lower slope. The blade core NL7-BC1 is a reference core
169 recovered in the middle slope, away from fluid venting structures. The lithological
170 description for those cores is presented in Fig. 5. Hemipelagic sediments in the Nile deep
171 sea fan correspond typically to reddish-brown foraminiferal and pteropod oozes (core
172 NL7-BC1; uppermost part of cores NL14-PC1/3). In contrast, dark-grey sediments are
173 encountered frequently at cold seep sites (core NL6-PC1; lower part of cores NL14-PC

174 1/3), which may contain small (mm- to cm- size) concretions of authigenic carbonates
175 (Fig. 5).
176
177 3.4. Sediment geochemistry and pore water analyses
178 The inorganic geochemical composition of authigenic carbonates and sediments was
179 determined by wavelength dispersive X-ray fluorescence (WD-XRF) analysis of fusion
180 beads or compressed powder pellets for major and trace elements, respectively. Both
181 total and oxidised (SO_4) sulphur contents of sediment samples were measured by XRF,
182 allowing the determination of reduced sulphur concentrations (e.g. pyrite) by subtraction.
183 Pore waters were extracted from core NL14-PC1 sediments by centrifuge. Dissolved
184 sulphate concentrations were measured in 1:10 diluted solutions by ion chromatography
185 with an accuracy better than 4%.
186
187 3.5. U/Th dating of authigenic carbonates
188 Bayon et al. (2007) reported ^{230}Th/U ages for a set of samples drilled across a
189 carbonate crust recovered from the middle slope (NL7-CC2 crust; see location in Fig. 4),
190 which provided evidence for continuous carbonate precipitation at that studied location
191 over the last ~ 5000 years at least. In this study, we performed additional U-Th isotope
192 measurements for two other carbonate crusts (NL6-CC1 and NL14-CC5; see location in
193 Figs. 3B,C), collected from carbonate ridges in the lower slope. NL6-CC1 and NL14-
194 CC5 crusts correspond to carbonate pavements characterized by a homogeneous matrix
195 of terrigenous sediment (silt, clay), foraminifers and nannofossils, cemented by fine-
196 grained aragonite (Gontharet et al., 2007).

197 Details on chemical and analytical procedures are presented elsewhere (Bayon et al.,
198 2007), and a brief description is given here. Selected areas of carbonate crusts were
199 hand-drilled carefully to obtain ~100 mg of carbonate powder. Carbonate samples were
200 spiked with a mixed $^{236}U/^{229}Th$ spike prior to sample digestion. U and Th were then
201 separated chemically using conventional anion exchange techniques. U and Th
202 concentrations and isotope ratios were measured by multiple collector inductively
203 coupled plasma mass spectrometry (MC-ICPMS) at the University of Oxford. Detrital
204 contamination was typically too high for allowing calculation of ages using the
205 conventional ^{230}Th age equation and required instead the use of isochron methods (e.g.
206 Bourdon et al., 2003). For this approach, a sediment end-member was defined as the
207 average of two sediments from the studied area (Bayon et al., 2007), assumed to be
208 representative of the sediment fraction incorporated within the carbonate crusts.
209
210 **4 – Results**
211 4.1. Morphology of the Central Nile Province
212 New geophysical data acquired during the Nautinil cruise and other recent Geosciences-
213 Azur expeditions allow to distinguish three distinct areas in the Central Nile Province,
214 which are described briefly below (Fig. 1; Fig. 2):
215
216 a) The upper slope (between ~ 500 and 700 m water depth), characterised by the presence
217 of a few large gas chimneys (up to 4 km in diameter) corresponding to the leakage of gas-
218 rich fluids from poorly sealed hydrocarbon reservoirs (e.g. North Alex; Fig. 1).
219 Numerous slides observed in deeper parts of the Central Nile Province initiate at the

location of the gas chimneys (Loncke et al., 2004). Note that one *Nautile* dive took place in this area (i.e. North Alex chimney) during the Nautinil cruise, but those results are discussed elsewhere (Dupré et al., 2007).

b) The middle slope (between ~ 700 and 1650 m water depth), characterised by a series of transparent acoustic bodies (debris-flow deposits) overlapping surface sediments in the lower slope (Fig. 2A). The most recent debris-flow deposits in this area are overlain by a thin hemipelagic cover (~ 0.5 m), which suggests recent deposition. Ship-borne multibeam backscatter imagery reveals the presence of a few highly reflective patches in this area (Loncke et al., 2004).

c) The lower slope (between ~ 1650 and 2200 m water depth), characterised by rough and chaotic seafloor morphology. The sedimentary cover is deformed by repeated undulations (i.e. a succession of elongated ridges and troughs), between 300 to 1500 m wide, sub-parallel to the slope (Figs. 1, 2A,C). Loncke et al. (2002) interpreted those undulations as a result of creep and gliding processes, rather than sediment waves created by bottom currents. Examination of 3.5 kHz profiles (Fig. 2A; Loncke et al., 2002) also suggests that some ridges observed in this area correspond to small rotated blocks. This deformed sedimentary cover is about 10 to 50 m thick and is underlain by debris-flow deposits (Fig. 2A). In core NLK11 (see location in Fig. 1), debris-flow deposits occur at sediment depths below 12 m (Fig. 5). A large number of highly reflective patches were identified in this area (Loncke et al., 2004), some of which were investigated during the Nautinil cruise (Figs. 1 and 2).

243

244 4.2. Fluid venting structures

245 Microbathymetric profiles and maps for sediment facies and carbonate crust occurrences
246 along each *Nautile* dive transect are shown in Figures 3 and 4, together with EM-300
247 Multibeam acoustic map (Fig. 3A) and side-scan sonar seafloor imagery (Fig. 4). Note
248 that only the dive NL7 area (middle slope area) was surveyed by the EdgeTech deep tow
249 sonar during the Mimes expedition. Combining geophysical data, *in situ* observation and
250 microbathymetric profiles, four types of fluid venting structures can be identified in the
251 lower slope and middle slope parts of the Central Nile province, which are described
252 below.

253

254 4.2.1. Carbonate ridges (lower slope)

255 Three carbonate-paved areas were discovered on the lower slope during the *Nautile*
256 dives, which correspond clearly to highly reflective patches (dark spots) on EM-300
257 multibeam mosaic (Fig. 3A). Microbathymetric profiles generated from the submersible
258 sensors reveal that they correspond to aligned carbonate mounds, up to ~ 500 m long and
259 5 m high (Fig. 3B,C). Clearly, these carbonate-paved areas occur on top of the elongated
260 ridges related to downslope mass movements (Fig. 2). Carbonate pavements were mainly
261 covered by hemipelagic sediments (Fig. 6A). Fractured carbonate pavements were
262 observed typically in topographically steep areas (Fig. 3B; Fig. 6B,C), often associated to
263 faults with orientations ~ N70 and N160.

264

265 4.2.2. Elongated sediment depressions or troughs (lower slope)

In situ observations show the occurrence of large elongated depressions (~100 m long; 3 m deep) with signs of intense bioactivity, which occur in the immediate vicinity of carbonate ridges. The bioactivity is documented by the presence of light grey shell-rich sediments associated with numerous bioturbation mounds (Fig. 6G). Those depressions correspond to those slope-parallel troughs associated with undulations (Fig. 2), identified previously on multibeam bathymetric maps (Loncke et al., 2004). During the *Nautile* dives, many faults were observed in sediments (Fig. 3; Fig. 6H), with directions parallel (~N70) or perpendicular (~N160) to the slope (Fig. 3).

4.2.3. Other carbonate-paved areas (middle slope)

Two large (~ 1 km^2) carbonate-paved areas with irregular shapes and partly covered by sediments were identified from the side-scan sonar data in the middle slope (i.e. the large high backscatter areas shown as white patches in Fig. 4). The southernmost edge of one of these structures was visited during *Nautile* dive NL7 (Fig. 4), which corresponds to unfractured massive carbonate pavements. Bathymetric data acquired during the *Nautile* dive did not provide any evidence of topographic irregularities associated with carbonate pavements at that location.

4.2.4. Pockmarks

Numerous pockmarks were observed during the *Nautile* dives, both in the lower and middle slope areas. Pockmarks correspond to sub-circular depressions on the seafloor of variable size (typically 3-20 m across and up to 3 m deep), which can be isolated or occur as clusters (Figs. 4 and 6E). In the lower slope, pockmarks were observed in close

289 vicinity to troughs (Fig. 3). Authigenic carbonate crusts occur typically in the central part
290 of pockmarks, forming in some cases chimney-like build-ups (Fig. 6F). Shell debris,
291 authigenic carbonate crusts and infilled burrows often accumulate within the depressions
292 (Fig. 6F). In contrast to the reddish-brown foraminiferal and pteropod oozes
293 characterising hemipelagic sediments on the Nile deep-sea fan (see reference core; Fig.
294 5), dark grey sediments were observed frequently in pockmarks (pushcore NL6-PC1; Fig.
295 5).
296
297 4.3. Biological observations
298 Several animal communities were observed during the *Nautile* dives in the two studied
299 areas. Vestimentiferan tubeworms (Polychaeta: Siboglinidae) were often present in close
300 association with carbonate crusts (Fig. 7), both in pockmarks and carbonate-paved areas.
301 Two morphotypes of siboglinids were distinguished after examination of photographs
302 and videos collected during the dives, but only one of them (assigned to the genus
303 *Lamellibrachia*; Webb, 1969) was sampled successfully (Fig. 7A).
304 Numerous small mussels (length < ~1 cm) were found on carbonate crusts and
305 associated sediments, occurring frequently inside small cavities within carbonate
306 deposits. Those mussels have been shown recently to harbour 6 distinct types of bacterial
307 symbionts, including sulphur- and methane-oxidizing bacteria, a diversity larger than
308 reported from any other bivalve to date (Duperron et al, 2008). They display
309 morphological similarities to *Idas modiolaeformis* (Sturany, 1896), a species reported at
310 other eastern Mediterranean cold seep sites (Olu-Le Roy et al., 2004). Additional fauna
311 associated with crusts includes anemones, serpulid polychetes and small galatheid crabs.

312 Empty bivalve shells were observed in carbonate-paved areas and pockmarks, but also in
313 those large depressions close to carbonate ridges (P. Briand & K. Olu-Le Roy, pers.
314 com.). These shells are similar to shells of *Isorropodon perplexum* (Vesycomyidae) and
315 *Thyasira striata* (Thyasiridae), reported previously in the Nile deep-sea fan (Sturany,
316 1896) and on Anaximander mud volcanoes (Olu-Le Roy et al. 2004). A few living
317 specimens of lucinids were sampled, which exhibit close morphological similarities to
318 *Lucinoma kazani* (Anaximander mud volcanoes; Salas and Woodside 2002) and *Myrtea*
319 *amorpha* (Mediterranean Ridge cold seeps; Olu-Le Roy et al. 2004). The former were
320 shown recently to harbour sulphur-oxidizing bacteria (Duperron et al, 2007).
321
322 4.4. Detection of gas seeps
323 Methane profiles acquired in the lower slope with the Capsum METS sensor along
324 selected dive transects are shown in Figs. 3B and C. Significant methane anomalies were
325 measured in bottom waters above the large depressions associated with bioturbation
326 mounds. Clearly, this shows that those troughs correspond to active sites of methane
327 seepage. In contrast, no (dives NL6) or weak (dive NL14) methane anomalies were
328 detected above carbonate-paved areas (Figs. 3B and C). In the middle slope, the Capsum
329 sensor did not detect any methane anomaly (not shown here), but evidence for active
330 fluid seepage is suggested by acoustic anomalies of side-scan sonar records of the water
331 column attributed to gas bubbles (S. Dupré, personal communication; not shown here).
332 One such acoustic gas anomaly was identified in close proximity to those large carbonate
333 structures with irregular shapes.

334 At pockmarks, seepage of methane-rich fluids was inferred frequently by the presence
335 of dark grey sediments (e.g. indicating the presence of an abundant organic fraction not
336 decomposed). Evidence for on-going anaerobic oxidation of methane and bacterial
337 sulphate reduction in one of those pockmarks was also given by a strong H_2S smell upon
338 opening of core NL6-PC1 (Fig. 5).
339
340 4.5. Pore water and sediment geochemistry
341 Down-core high resolution profiles of CaO (wt. %), reduced and oxidized sulfur (wt.
342 %) and barium (ppm) contents in sediment from push-cores NL14-PC1 and NL14-PC3
343 are presented in Fig. 8. Dissolved sulphate concentrations in pore waters (for core NL14-
344 PC1 only) are also reported in Fig. 8. Pore water SO_4^{2-} concentrations are quasi-constant
345 down to ~17 cm depth, with values (~ 30 mM) close to seawater concentrations.
346 In contrast to dissolved SO_4^{2-} concentrations, S concentrations in solid sediment
347 phases increase from just a few centimeters (~ 7 cm) below the sediment/water interface
348 (Fig. 8). In core NL14-PC1, enrichments of Ba and reduced S are related to the presence
349 of barite (barium sulphate) and pyrite (iron sulfide), respectively. Mineralogical analyses
350 and microscope observations reveal that authigenic gypsum (calcium sulphate) is also
351 present within sediments.
352
353 4.6. Carbonate ^{230}Th/U ages
354 U-Th data for the two carbonate crusts analysed are listed in Table 2. Only one
355 meaningful age was obtained for those lithified carbonate samples collected on the
356 carbonate ridges (Table 2). This is due to an important ^{230}Th detrital contamination in

357 those clay-rich samples. The calculated age for sample NL14-CC5 is ~ 7.9 ± 1.4 ka
358 (Table 2).
359
360 **5 – Discussion**
361 5.1. Deformation style in the Central Nile margin
362 Significant differences were observed between the lower slope and the middle slope,
363 which are summarised in Table 3. In the lower slope, downslope mass movements lead
364 to formation of elongated ridges and troughs parallel to the slope (Loncke et al., 2002).
365 Observation of numerous fractures in sediments during the *Nautile* dives provides direct
366 evidence that active mass gravity processes occur in the lower slope. The presence of
367 similar ridges and troughs at the base of continental margins has been extensively
368 described in the literature (e.g. Mulder and Cochonat, 1996; van Weering et al., 1998;
369 Lee and Chough, 2001; Gay et al., 2004). In the case of creep and downslope gliding,
370 gravitational processes create typically two distinct structural domains: an extensional
371 domain in the upper slope and a compressive domain located downslope (e.g. Allen,
372 1985; Pickering et al., 1989; Stow, 1994). In most cases, ridges and troughs form in the
373 distal compressive parts of creeping or gliding sediment masses. By analogy, the lower
374 slope on the Central Nile deep-sea fan could also correspond to a regional compressive
375 domain. However, the occurrence of small rotated blocks in the lower slope indicates
376 that extensional deformation takes place instead in this area, leading to faulting and
377 associated rotated blocks. Most probably, it is likely that creeping of surface sediments
378 in this lower slope domain also induces local compression, which could contribute, at
379 least to some extent, to the formation of ridges and troughs.

In contrast to the lower slope, there is no direct evidence for active deformation processes taking place in the middle slope area. Most probably, the evidence that debris-flow deposits accumulated in the middle slope overlap surface sediments in the lower slope indicates that those two domains are decoupled.

5.2. Temporal evolution of fluid circulation

In cold seep environments, reduction of sulphate in pore waters is closely related to methane oxidation (Niewöhner et al., 1998; Borowski et al., 1999). The depth at which sulphate reduction occurs in sediments is controlled primarily by the upward flux of methane, being closer to the seafloor for high methane fluxes (Niewöhner et al., 1998; Borowski et al., 1999). Information on the temporal evolution of fluid venting at any site can be obtained by comparing pore water data (which give information on present-day fluid circulation) and solid sediment geochemical data (which may provide an integrated record of fluid seepage over the last few thousand years). In core NL14-PC1, the constant dissolved sulphate profile indicates that sulphate reduction does not proceed in the top sediment layer (~ 0-20 cm) at present. This suggests that methane-rich fluids probably do not circulate in sub-surface sediments at this location.

In contrast, the presence of authigenic sulphate (oxidized S) and sulfide (reduced S) minerals within sediment cores collected at carbonate ridges implies that reduction of pore-water sulphate was active at these sediment depths in the recent past. The dark grey sulfur- and barium-rich sediment layer in cores NL14-PC1/3 probably does not correspond to the Holocene Sapropel layer S1 (e.g., Olausson, 1961), which is buried at deeper sediment depths in the studied area (> 15 cm in our reference push-core NL7-

403 BC1; Fig. 5). The occurrence of S-rich minerals in NL14-PC1/3 sediments is probably
404 related to oxidation of methane-rich fluids at that location in the recent past. At present,
405 cold seep settings where sulphate reduction proceeds at only a few centimeters below the
406 seafloor correspond to sites characterized by active fluid advection (e.g. see Haese et al.,
407 2003 and references therein).

408 Absolute dating of authigenic carbonates with U-series also provides a means for
409 reconstructing the evolution of cold seeps and associated fluid circulation through time
410 (Teichert et al., 2003; Bayon et al., 2007). Certainly, additional U-Th isotope
411 measurements would be needed to better constrain any spatial and temporal variations of
412 fluid circulation activity in the lower slope. However, the U-Th age (~ 8 kyr BP)
413 calculated for crust NL14-CC5 suggests that carbonate precipitation and hence fluid
414 seepage was active at the studied carbonate ridge in the early Holocene. Taken together,
415 our U-Th data and sediment geochemical profiles suggest therefore that the activity of
416 fluid venting at carbonate ridge locations may have decreased over a recent period.

417

418 5.3. The origin of fluids

419 Fluids expelled at cold seeps on the Nile deep-sea fan may derive from shallow and/or
420 deep sediment sources. Potential deep fluid sources include messinian and pre-messinian
421 thermogenic hydrocarbon reservoirs (Abdel Aal et al., 2000; Samuel et al., 2003; Loncke
422 et al., 2004). During the Nautinil expedition, the discovery of brine lakes on the seafloor
423 (Menes Caldera, Western Nile province; Huguen et al., in revision) has provided clear
424 evidence that fluids passing through or originating from deep evaporite deposits could be
425 emitted on the seafloor in the Nile Delta area. Shallow fluid sources at cold seeps are

426 most often related to formation of biogenic methane in superficial sediment layers; a
427 consequence of the microbial degradation of organic matter during early diagenetic
428 processes. Several organic-rich sediment layers (sapropels) have accumulated in Eastern
429 Mediterranean basins during the Late Quaternary period (e.g., Olausson, 1961; De Lange
430 and Ten Haven, 1983; Rossignol-Strick et al., 1982), which represent potential sources of
431 methane-rich fluids to cold seeps in the Nile deep sea fan area. Fine-grained turbidites
432 deposited on the deep-sea fan during the Late Quaternary may represent an additional
433 source of biogenic methane. None of the data presented in this study can be used to
434 discriminate the origin of fluids in the Central Nile area. However, stable isotope
435 measurements ($\delta^{13}C$ and $\delta^{18}O$) on authigenic crusts collected during the Nautinil
436 expedition (Gontharet et al., 2007) suggest that the fossil carbon source involved in
437 carbonate precipitation in this area derives from biogenic methane primarily (i.e. a
438 shallow source).
439
440 5.4. Formation mode of fluid-escape structures and links with sediment deformation
441 5.4.1. Lower slope
442 One major result of this study is the close relationship between slope parallel elongated
443 ridges/troughs and the occurrence of fluid-escape structures (see Fig. 9; Table 3). In the
444 lower slope, carbonate-paved areas are located clearly on top of ridges, whereas methane
445 venting occurs above troughs (Fig. 9). It is very likely that gravity processes and
446 deformation in the lower slope have created preferential pathways for fluid migration and
447 gas escape. The large depressions or troughs, characterized by intense bioactivity and
448 active methane venting, corresponds most probably to the present-day seafloor

449 expression of those preferential pathways (e.g. faults) related to sediment deformation
450 (Fig. 9). Pockmarks observed in close vicinity to the troughs could form from excess
451 volumes of fluids periodically migrating upslope from the troughs, possibly aided by the
452 creation of migration pathways along fractures (Fig. 9).

453 At present, it is likely that carbonate precipitation occurs within sediments in those
454 depressions associated to active methane venting. Instead, we propose that carbonate
455 pavements emplaced on top of ridges were outcropped on the seafloor in response to
456 sediment instability, *after* initial formation of carbonate crusts. The exposure of those
457 carbonate pavements could be due either to compressional deformation as pressure ridges
458 or, alternatively, be related to faulting associated with the rotated blocks. This
459 exhumation process would be in agreement with the presence of intensively fractured
460 carbonate crusts on top of those ridges. Carbonate ridges would hence correspond to
461 'paleo-troughs' (i.e. ancient sites of active fluid venting). Our geochemical results
462 suggest that fluid seepage at those ridges has decreased most probably since the early
463 Holocene (see section 5.2). Most likely, this indicates that slope instability may induce a
464 change in fluid flow conditions at any given location; from focused flow to diffuse flow
465 for the case of those carbonate ridges. The persistence of seep habitats on top of ridges at
466 present would hence be related to pervasive microseepage only.
467
468 Other carbonate ridges were discovered recently on the continental slope off Norway
469 (Hovland et al., 2005), though in a different geological setting (e.g. proximity to gas
470 hydrate reservoirs). Hovland et al. (2005) proposed that such ridges were formed during
471 catastrophic fluid-flow events, in response to abrupt breaking of carbonate seals above

472 preferential fluid pathways. In the Central Nile province, however, observation that
473 carbonate ridges occur only on one side of those large sediment depressions (see
474 bathymetric profile in Figs. 3B and C) argues against such a formation by catastrophic
475 fluid flow event. Therefore, our preferred explanations remain that: 1) fluid migration is
476 controlled by slope instability in the lower slope, and 2) sediment gliding is responsible
477 for formation of carbonate ridges.
478
479 During the last few hundred thousand years, sediment mass-wasting has been active in
480 the Nile deep sea fan, leading to deposition of a series of debris-flows and turbidites
481 (Ducassou et al., 2007). It is likely that sediment accumulation on the middle and lower
482 slopes has led, to some extent, to compaction/dewatering in sub-surface sediments,
483 generating ultimately excess pore water pressure and fluid migration. Investigation of
484 core NLK11 shows that sediments deposited above those debris-flow deposits (i.e. the
485 top ~ 12 m of core NLK11) exhibit vertical pipes filled with fluidised sediments, which
486 correspond to fluid migration structures (Fig. 5). In contrast, sediments associated with
487 debris-flow deposits are highly compacted. One hypothesis would be that the upper
488 surface of debris-flow deposits act as a décollement layer, along which fluids would
489 migrate preferentially. The presence of such a décollement layer at a few meters below
490 the seafloor would favour both sediment instabilities (i.e. creeping) and fluid seepage in
491 the lower slope (Fig. 9).
492
493 5.4.2. Middle slope

Significant differences in e.g. surface, morphology, fracturation have been observed between carbonate-paved areas from the lower and middle slopes (see section 4.2), indicating that they were formed most probably through distinct processes. U/Th isotope ages calculated on authigenic carbonates recovered from the middle slope (Bayon et al., 2007) showed that fluid emission in this area (at least in that carbonate-paved area explored during dive NL7) has remained active for the last 5,000 years at least. This suggests that the middle slope has remained stable (i.e. no major slope instability) during that period. In contrast with the lower slope, the absence of any significant preferential conduits and/or faulting within surface sediments in this area may provide possibilities for broad diffusive, perhaps not focused, but permanent fluid venting through time.

5. Conclusions

Fluid venting is active on the Central Nile margin, as demonstrated by the observation of fluid-related structures (pockmarks, carbonate pavements), abundant associated chemosynthetic communities and the detection of bottom-water methane anomalies. Detailed investigations of cold seeps from two distinct areas in the Central Nile province indicate a link between fluid seepage and sediment instability.

The lower slope from 1650 m to 2200 m water depth is a zone of regional sediment creeping, where active gravitational processes create a series of elongated slope-parallel ridges and depressions. Fossil carbonate ridges up to 5m high occur on top of those slope-parallel ridges, whereas the deep depressions correspond to areas of active fluid flow. The middle slope from 700 m to 1650 m water depth corresponds to an area

517 recently covered by debris flow deposits, which overlap surface sediments in the lower
518 slope. In contrast with the lower slope, it shows no signs of sediment creeping, but
519 exhibits large patchy areas (~1 km^2) of carbonate pavements associated to broad and
520 more diffuse fluid flow.

521 We propose that sediment instability in the lower slope area creates preferential
522 pathways for focused fluid flow and leads to the exposure of carbonate ridges. Evidence
523 that debris-flow deposits buried under the destabilized sedimentary cover in this area are
524 highly compacted may suggest that the top of this debris-flow unit acts as a décollement
525 layer, along which fluids would migrate preferentially and, in turn, favor sediment
526 gliding. Overall, our results have general implications for understanding the processes
527 controlling methane fluxes at continental margins, and how slope instability may
528 contribute to methane release into the water column.

529

530

531 **Acknowledgements**

532 We thank the Captains, the officers and crews of R/V *Atalante* and R/V *Pelagia*, the
533 pilots and technicians of *Nautile,* and members of the Nautinil and Mimes scientific
534 parties for their assistance at sea. We are grateful to P. Briand (Ifremer) for his help in
535 identifying biological specimens. A. Mason (U. Oxford) is thanked for assistance during
536 U/Th analyses. Two anonymous reviewers are thanked for their comments and
537 suggestions. The Nautinil and Mimes expeditions were funded by IFREMER and the
538 Netherlands Organization for Scientific research (NWO), respectively, as part of the
539 MEDIFLUX Project (EUROMARGINS–ESF programme).

References

Abdel Aal, A., El Barkooky, A., Gerrits, M., Meyer, H., Schwander, M., Zaki, H.A., 2000. Tectonic evolution of the Eastern Mediterranean basin and its significance for hydrocarbon prospectivity in the ultradeepwater of the Nile delta. The Leading Edge, 1086–1102.

Allen, J.R.L., 1985. Principles of physical sedimentology. Allen and Unwin, London, 272 pp.

Bayon, G., Henderson, G.M., Bohn, M., Gontharet, S., Pierre, C., 2007. U-Th stratigraphy of a cold seep carbonate crust. Geochim. Cosmochim. Acta 71, 15, Supplement 1, A68-A68.

Bellaiche, G., Loncke, L., Gaullier, V., Mascle, J., Courp, T., Moreau, A., Radan, S., Sardou, O., 2001. Le cône sous-marin du Nil et son réseau de chenaux profonds: Nouveaux résultats (campagne Fanil). C. Rd. Ac. Sci., Paris 333, 399–404.

Borowski, W. S., Paull, C. K., Ussler III, W., 1999. Global and local variations of interstitial sulphate gradients in deep-water, continental margin sediments: Sensitivity to underlying methane and gas hydrates. Mar. Geol. 159, 131-154.

Bourdon, B., Henderson, G. M., Lundstrom, C. C., Turner, S. P., 2003. Uranium-series geochemistry. Rev. Min. Geochem. 52, 656 pp.

de Lange, G.J., Ten Haven, H.L., 1983. Recent sapropel formation in the eastern Mediterranean. Nature 305, 797-798.

Dimitrov, L., Woodside, J., 2003. Deep sea pockmarks environments in the eastern Mediterranean. Mar. Geol. 195, 263–276.

562 Ducassou, E., Capotondi, L., Murat, A., Bernasconi, S. M., Mulder, T., Gonthier, E.,
563 Migeon, S., Duprat, J., Giraudeau, J., Mascle, J., 2007. Multiproxy Late Quaternary
564 stratigraphy of the Nile deep-sea turbidite system — Towards a chronology of deep-
565 sea terrigeneous system. Sedim. Geol. 200, 1-13.
566 Duperron, S., Fiala-Médioni, A., Caprais, J.-C., Olu, K., Sibuet, M., 2007. Evidence for
567 chemoautotrophic symbiosis in a Mediterranean cold seep clam (Bivalvia:
568 Lucinidae): comparative sequence analysis of bacterial 16S rRNA, APS reductase
569 and RubisCO genes. FEMS Microbiol. Ecol. 59, 64-70.
570 Duperron, S., Halary, S., Lorion, J., Sibuet, M., Gaill, F., 2008. Unexpected co
571 occurrence of 6 bacterial symbionts in the gill of the cold seep mussel Idas sp.
572 (Bivalvia: Mytilidae). Environ. Microbiol. 10(2), 433-445.
573 Dupré, S., Woodside, J., Foucher, J.-P., de Lange, G., Mascle, J., Boetius, A., Mastalerz,
574 V., Stadnitskaia, A., Ondreas, H., Huguen, C., Caprais, J.-C., Gontharet, S., Loncke,
575 L., Deville, E., Niemann, H., Fiala-Medioni, A., Dählmann, A., Prinzhofer, A.,
576 Sibuet, M., Pierre, C., Sinninghe Damsté, J., 2007. Seafloor geological studies above
577 active gas chimneys off Egypt (Central Nile Deep Sea Fan). Deep-Sea Res. I 54,
578 1146-1172.
579 Gaullier, V., Mart, Y., Bellaiche, G., Mascle, J., Vendeville, B., Zitter, T., the Prismed
580 Scientific Party, 2000. Salt tectonics in and around the Nile deep sea fan : insights
581 from the Prismed II cruise. In: Vendeville, B., Mart, Y., Vigeresse, J.L. (eds.) Salt,
582 Shale and Igneous diapirs in and around Europe. Geological Society, London, Spec.
583 Pub. 174, 110-129.

584 Gay, A., Lopez, M., Cochonat, P., Sermondadaz, G., 2004. Polygonal faults–troughs
585 system related to early stages of compaction—Upper Miocene to present sediments of
586 the Lower Congo Basin. Basin Res. 16, 101–116.
587 Gay, A., Lopez, M., Cochonat, P., Séranne, M., Levaché, D., Sermondadaz, G., 2006.
588 Isolated seafloor pockmarks linked to BSRs, fluid chimneys, polygonal faults and
589 stacked Oligocene–Miocene turbiditic palaeochannels in the Lower Congo Basin.
590 Mar. Geol. 226, 25-40.
591 Gontharet, S., Pierre, C., Blanc-Valleron, M.M., Rouchy, J.M., Fouquet, Y., Bayon, G.,
592 Foucher, J.P., Woodside, J., Mascle, J., the Nautinil scientific party, 2007. Nature and
593 origin of the diagenetic carbonate crusts and concretions from mud volcanoes and
594 pockmarks of the Nile deep-sea fan (eastern Mediterranean sea). Deep-Sea Res. II
595 54, 1291-1316.
596 Haese, R. R., Meile, C., van Cappellen, P., de Lange, G. J., 2003. Carbon geochemistry
597 of cold seeps: Methane fluxes and transformation in sediments from Kazan mud
598 volcano, eastern Mediterranean Sea. Earth Planet. Sci. Let. 212, 361-375.
599 Hovland, M., Judd, A.G., 1988. Seabed Pockmarks and Seepages: Impact on Geology,
600 Biology and Marine Environment vol. 293, Graham and Trotman, London, 565 pp.
601 Hovland, M., Gardner, J.V., Judd, A.G., 2002. The significance of pockmarks to
602 understanding fluid flow processes and geohazards. Geofluids 2, 127–136.
603 Hovland, M., Svensen, H., Forsberg, C.F., Johansen, H., Fichler, C., Fosså, J.H., Jonsson,
604 R., Rueslåtten, H., 2005. Complex pockmarks with carbonate-ridges off mid-Norway:
605 Products of sediment degassing. Mar. Geol. 218, 191-206.

606 Huguen, C., Foucher, J.-P., Mascle, J., Ondreas, H., Thouement, M., Gontharet, S.,
607 Stadnitskaia, A., Pierre, C., Bayon, G., Loncke, L., Boetius, A., Bouloubassi, I., de
608 Lange, G., Caprais, J.-C., Fouquet, Y., Woodside, J., and the NAUTINIL Scientific
609 Party, 2008. Menes Caldera, a highly active site of brine seepage in the Eastern
610 Mediterranean Sea: “in situ” observations from the Nautinil expedition (2003).
611 Marine Geology (EUROMARGINS Special Issue, **This volume**).
612 Judd, A.G., Hovland, M., 2007. Seabed Fluid Flow, the impact on geology, biology and
613 the marine environment. Cambridge University Press, 475 pp.
614 Kennett, J. P., Cannariato, K. G., Hendy, I. L., Behl, R. J., 2002. Methane hydrates in
615 quaternary climate change: the clathrate gun hypothesis. Am. Geophys. Union, 216
616 pp.
617 Lastras, G., Canals, M., Urgeles, R., Hughes-Clarke, J.-E., Acosta, J., 2004. Shallow
618 slides and pockmark swarms in the Eivissia Channel, western Mediterranean Sea.
619 Sedimentology 51, 1–14.
620 Lee, S.H., Chough, S.K., 2001. High-resolution (2±7 kHz) acoustic and geometric
621 characters of submarine creep deposits in the South Korea Plateau, East Sea.
622 Sedimentology 48, 629-644.
623 Loncke, L., Gaullier, V., Bellaiche, G. and Mascle, J., 2002. Recent depositional patterns
624 of the Nile Deep-Sea Fan from echo-character mapping. AAPG Bull. 86, 1165–1186.
625 Loncke, L., Mascle, J., Fanil Science Party, 2004. Mud volcanoes, gas chimneys
626 pockmarks and ridges in the Nile deep-sea fan (Eastern Mediterranean): geophysical
627 evidences. Mar. Petrol. Geol. 21, 669–689.

628 Loncke, L., Gaullier, V., Mascle, J., Vendeville, B., Camera, L., 2006. The Nile deep-sea
629 fan : An example of interacting sedimentation, salt tectonics, and inherited subsalt
630 paleotopographic features. Mar. Petrol. Geol. 23, 297-315.
631 Mascle, J., Benkhelil, J., Bellaiche, G., Zitter, T., Woodside, J., Loncke, L. and Prismed
632 II scientific party, 2000. Marine geological evidence for a Levantine–Sinai plate, a
633 missing piece of the Mediterranean puzzle. Geology 28, 779–782.
634 Maslin, M.A., Owen, M., Day, S., Long, D., 2004. Linking continental slope failure to
635 climate change: Testing the Clathrate Gun Hypothesis. Geology 32, 53-56.
636 Mienert, J., 2004. COSTA—continental slope stability: major aims and topics. Mar.
637 Geol. 213, 1-7.
638 Mienert, J., Vanneste, M., Bünz, S., Andreassen, K., Haflidason, H., Sejrup, H.P., 2005.
639 Ocean warming and gas hydrate stability on the mid-Norwegian margin at the
640 Storegga Slide. Mar. Petrol. Geol. 22, 233-244
641 Mulder, T., Cochonat, P., 1996. Classification of offshore mass movements. J. Sedim.
642 Res. 66, 43-57.
643 Niewöhner, C., Hensen, C., Kasten, S., Zabel, M., Schulz, H. D., 1998. Deep sulphate
644 reduction completely mediated by anaerobic methane oxidation in sediments of the
645 upwelling area off Namibia. Geochim. Cosmochim. Acta 62, 455-464.
646 Nisbet, E.G., 2002. Have sudden large releases of methane from geological reservoirs
647 occurred since the Last Glacial Maximum, and could such releases occur again? Phil.
648 Trans. R. Soc. Lond. A 360, 581-607.
649 Olausson, E., 1961. Studies of deep sea cores. Reports of Swedish Deep-Sea expeditions
650 1947-1948, 8, 336-391.

651 Olu-Le Roy, K., Sibuet, M., Fiala-Médioni, A., Gofas, S., Salas, C., Mariotti, A.,
652 Foucher, J.P., Woodside, J., 2004. Cold seep communities in the deep eastern
653 Mediterranean Sea: composition, symbiosis and spatial distribution on mud
654 volcanoes. Deep-Sea Res. I 51, 1915-1936.
655 Paull, C.K., Ussler III, W., Dillon, W.P., 2000. Potential role of gas hydrate
656 decomposition in generating submarine slope failures. In: Max, M.D. (Ed.), Natural
657 Gas Hydrate in Oceanic and Permafrost Environments, Kleuwer Acad. Publishers,
658 Dordrecht, 149–156.
659 Paull, C., Ussler III, W., Maher, N., Greene, H.G., Rehder, G., Lorenson, T., Lee, H.,
660 2002. Pockmarks off Big Sur, California. Mar. Geol. 181, 323–335.
661 Pickering, K.T., Hiscott, R.N., and Hein, F.J., 1989. Deep marine environments. Harper-
662 Collins, London, 416 pp.
663 Rossignol-Strick, M., Nesteroff, W.D., Olive, P., Vergnaud-Grazzini C., 1982. After the
664 deluge: Mediterranean stagnation and sapropel formation. Nature 295, 105-110.
665 Salas, C., Woodside, J., 2002. *Lucinoma kazani* n. sp. (Mollusca: Bivalvia): evidence of
666 a living benthic community associated with a cold seep in the Eastern Mediterranean
667 Sea. Deep-Sea Res. I 49, 991-1005.
668 Salem, R., 1976. Evolution of Eocene–Miocene sedimentation patterns in parts of
669 Northern Egypt. AAPG Bull. 60, 34–64.
670 Samuel, A., Kneller, B., Raslan, S., Sharp, A. and Parsons, C., 2003. Prolific deep-marine
671 slope channels of the Nile delta, Egypt. AAPG Bull. 87, 541–560.
672 Sardou, O., Mascle, J., 2003. Cartography by multibeam echo-sounder of the Nile deep-
673 sea Fan and surrounding areas (2 sheets). Special publication CIESM, Monaco.

674 Sowers, T., 2006. Late Quaternary atmospheric CH4 isotope records suggests marine
675 clathrates are stable. Nature 311, 838-840.
676 Stow, D.A.V., 1994. Deep-sea processes of sediment transport and deposition. In: Pye, K.
677 (Ed.), Sediment Transport and Depositional Processes. Blackwell, London, pp. 257-
678 293.
679 Sturany, R., 1896. Zoologische Ergebnisse VII. Mollusken I (Prosobranchier und
680 Opisthobranchier; Scaphopoden; Lamellibranchier) gesammelt von S.M. Schiff
681 "Pola" 1890-1894. Denkschriften der Kaiserlichen Akademie der Wissenschaften,
682 Mathematische-Naturwissenschaftlischen Classe 63, 1-36, pl.1-2.
683 Teichert, B. M. A., Eisenhauer, A., Bohrmann, G., Haase-Schramm, A., Bock, B., Linke,
684 P., 2003. U/Th systematics and ages of authigenic carbonates from Hydrate Ridge,
685 Cascadia Margin: recorders of fluid flow variations. Geochim. Cosmochim. Acta 67,
686 3845-3857.
687 Trincardi, F., Cattaneo, A., Correggiari, A., Ridente, D., 2004. Evidence of soft sediment
688 deformation, fluid escape, sediment failure and regional weak layers within the late
689 Quaternary mud deposits of the Adriatic Sea. Mar. Geol. 213, 91-119.
690 Ussler III, W., Paull, C.K., Boucher, J., Friederich, G.E., Thomas, D.J., 2003. Submarine
691 pockmarks: a case study from Belfast Bay, Maine. Mar. Geol. 202, 175–192.
692 van Weering, T.C.E., Nielsen, T., Kenyon, N.H., Akentieva, A.K., Kuijpers, A. 1998.
693 Large Submarine slides at the NE Faroe continental margin. In: Stoker, M., Evans,
694 D., and Cramp, R. (Eds.), Geological Processes on Continental Margins:
695 Sedimentation, Mass-Wasting and Stability. Geological Society London Special
696 Publications 129, pp. 5-17.

697 Vogt, P.R., Gardner, J., Crane, K., Sundvor, E., Bowles, F., Cherkashev, G., 1999.
698 Ground-truthing 11- to 12-kHz side-scan sonar imagery in the Norwegian–Greenland
699 Sea. Part I: pockmarks on the Vestnesa Ridge and Storegga slide margin. Geo Mar.
700 Lett. 19, 97–110.
701 Webb, M., 1969. *Lamellibrachia barhami* gen. nov. sp. nov., (Pogonophora) from the
702 northeast Pacific. Bull. Mar. Sci. 19, 18–47.

703 **Figure Captions**

704

705 **Figure 1**: Bathymetric map of the Nile deep-sea fan (Sardou and Mascle, 2003) and
706 distribution of fluid-escape structures (Loncke et al., 2004) showing the two sites
707 investigated with the *Nautile* submersible, at 2100 m depth (lower slope) and 1650 m
708 depth (middle slope). Note the presence of elongated ridges sub-parallel to the slope
709 (direction ~ N70) in the lower slope of the Central Province.

710

711 **Figure 2**: (A) 3.5-kHz sub-bottom profile perpendicular to the slope in the Central Nile
712 Province (see Fig. 1 for NL2-6 trackline position). (B,C) Shaded bathymetric maps of
713 the two sites investigated in the Central Nile Province with position of the *Nautile*
714 transects (see location of sites in Fig. 1). (B) Middle slope, dive NL7, 1650 m water
715 depth; (C) Lower slope, dives NL6 and NL14, 2100 m water depth. Note the marked
716 morphological contrast between the middle slope and the lower slope. The lower slope is
717 characterised by a rough and morphological seafloor morphology, which exhibits
718 repeated elongated ridges and depressions parallel to the slope.

719

720 **Figure 3**: Seafloor observations of fluid-escape structures in the lower slope domain.
721 (A) Multibeam seafloor acoustic imagery showing the distribution of highly reflective
722 patches (dark spots) with indication of the *Nautile* transects (see location of sites in Fig.
723 1). (B,C) Maps for sediment and carbonate facies, microbathymetric profiles and
724 bottom-water methane anomalies recorded along the dive transects. Fault positions and
725 sampling sites for sediment cores and carbonate crusts are also shown.

Figure 4: Side-scan sonar image of the seafloor in the middle slope showing the presence of large carbonate paved-areas with indication of the *Nautile* transect (see location in Fig. 1). Sampling sites for sediment cores and carbonate crusts collected during the dive are also reported.

Figure 5: Lithological description of sediment cores recovered during the submersible dives. Push cores NL6-PC1, NL14-PC1 and NL14-PC3 were collected in the lower slope, in fluid-venting areas (pockmark, carbonate ridges). Box core NL7-BC1 was recovered in the middle slope, away from any fluid-escape structure. The location of these cores is shown in Figs. 1, 3B,C, and 4.

Figure 6: Seafloor bottom photographs of fluid-escape structures. (A) Carbonate pavements partly covered by thin sediments (carbonate ridge; lower slope). (B) Fractured carbonates on a carbonate ridge (lower slope). (C) Fracture on a carbonate ridge (lower slope). (D) Non fractured massive carbonate pavement (middle slope). (E) Small pockmark (~ 3 m across) in the lower slope. Note the presence of authigenic carbonates, grey anoxic sediments and vestimentiferan tubeworms. (F) Large pockmark (~ 25 m across) exhibiting two carbonate chimneys and a dense network of infilled burrows (middle slope). The central part of the pockmark corresponds to accumulated debris of dead shells, authigenic carbonates and burrows. (G) Shell-rich sediments and bioturbation mounds in one of those troughs (large seafloor depression) related to gravity tectonics

748 (lower slope). (H) Fault in hemipelagic sediments away from fluid-escape structures
749 (lower slope). White scale bars correspond to ~ 1 m.
750
751 **Figure 7**: Vestimentiferan tubeworms associated with carbonate crusts. (A) First
752 morphotype observed, assigned preliminarily to the genus *Lamellibrachia* (dive NL7;
753 middle slope). (B) Second morphotype observed, but not collected (dive NL6; lower
754 slope). Note that the morphology of the chitinous tube differs from that of the first morphotype.
755 White scale bars correspond to ~ 20 cm.
756
757 **Figure 8**: Down-core profiles of CaO (wt%), $S_{oxidized}$ (wt%), $S_{reduced}$ (wt%), Ba (ppm)
758 for push-cores NL14-PC1 and NL14-PC3 taken at a carbonate ridge (lower slope, see
759 location in Figs. 3B and C). Dissolved pore water SO_4^{2-} (mM) contents are also plotted
760 for core NL14-PC1. Enrichments of oxidized/reduced sulphur and barium in solid
761 sediment phases indicate that reduction of dissolved sulphates has been active at these
762 locations in the recent past. In contrast, the flat dissolved SO_4^{2-} profile, with seawater-
763 like values, shows that sulphate reduction does not take place in sub-surface sediments at
764 present.
765
766 **Figure 9**: Conceptual model linking fluid seepage and sediment deformation in the lower
767 slope. Active gravitational processes (creep and/or gliding) create a series of elongated
768 slope-parallel sediment ridges and depressions in the lower slope. Sediment instability
769 leads to exhumation of fractured carbonate pavements on top of ridges, which correspond
770 to 'fossil' vent sites. The exhumation of those carbonate ridges can be due either to

771 compressional deformation (i.e. creep) or be related to faulting associated with rotated
772 blocks (i.e. gliding). The depressions correspond instead to preferential pathways for
773 focused fluid flow. The top of debris-flow deposits (highly compacted) buried under the
774 destabilized sediment cover could act as a décollement layer along which fluids would
775 migrate preferentially, favouring in turn sediment gliding.
776

Table 1. Positions and water depths of the cores and carbonate crusts investigated

Core / Carbonate	Description	Length (m)	Water depth (m)	Latitude N	Longitude E
Sediment cores					
NL6-PC1	Push core	0.36	2115	32°38.14'	29°56.12'
NL14-PC1	Push core	0.35	2116	32°38.33'	29°55.80'
NL14-PC3	Push core	0.25	2130	32°38.44'	29°54.98'
NLK11	Kullenberg	14	2207	32°40.99'	29°54.00'
NL7-BC1	Blade core	0.15	1623	32°30.50'	30°23.09'
Carbonate crusts					
NL6-CC1	lithified crust		2132	32°38.38'	29°54.87'
NL14-CC5	lithified crust		2130	32°38.44'	29°54.98'
NL7-CC2	porous crust		1686	32°31.61'	30°21.16'

Table 2. U-Th data for authigenic carbonates

Sample	Depth (cm)	^{238}U (ppm)	^{230}Th (ppt)	($^{230}Th/^{232}Th$)	$\delta^{234}U_{(0)}$	Isochron age (ka)
NL14-CC5	0.5	2.997 ± 0.004	28.67 ± 0.14	2.44 ± 0.01	128.7 ± 1.7	-
'	2	5.158 ± 0.006	17.15 ± 0.04	3.62 ± 0.01	144.2 ± 1.7	7.9 ± 1.4
NL6-CC1	2	3.702 ± 0.004	35.29 ± 0.15	2.52 ± 0.01	129.3 ± 1.7	-

Table 3. Geological setting and fluid-vent structures in the lower and middle slope

	Lower slope	Middle slope
Geological setting	▪ Debris-flow deposits overlain by a 'thick' creeping hemipelagic cover (~15 m)	▪ Debris-flow deposits overlain by 'thin' hemipelagic cover (~ 0.5 m)
Seafloor surface	▪ Rough (ridges and troughs)	▪ Flat
Gravitational processes	▪ Active creeping processes leading to formation of ridges and throughs ▪ Extensional regime mainly (rotated blocks) ▪ Probably local compressive ridges distally and above irregularities of decollement plane	▪ Not active at present ▪ Uniformaly disorganised debris-flow deposits
Fluid-vent structures	▪ Carbonate ridges (~500 m long) associated with compressional ridges ▪ Throughs (methane emission) ▪ Small pockmarks	▪ Large carbonate-paved areas (> 1 km^2) with irregular shapes ▪ Pockmarks
Degree of seepage activity	▪ Reduced activity at carbonate ridges ▪ Active methane venting above furrows	▪ Continuous activity for at least the last ~5 kyr

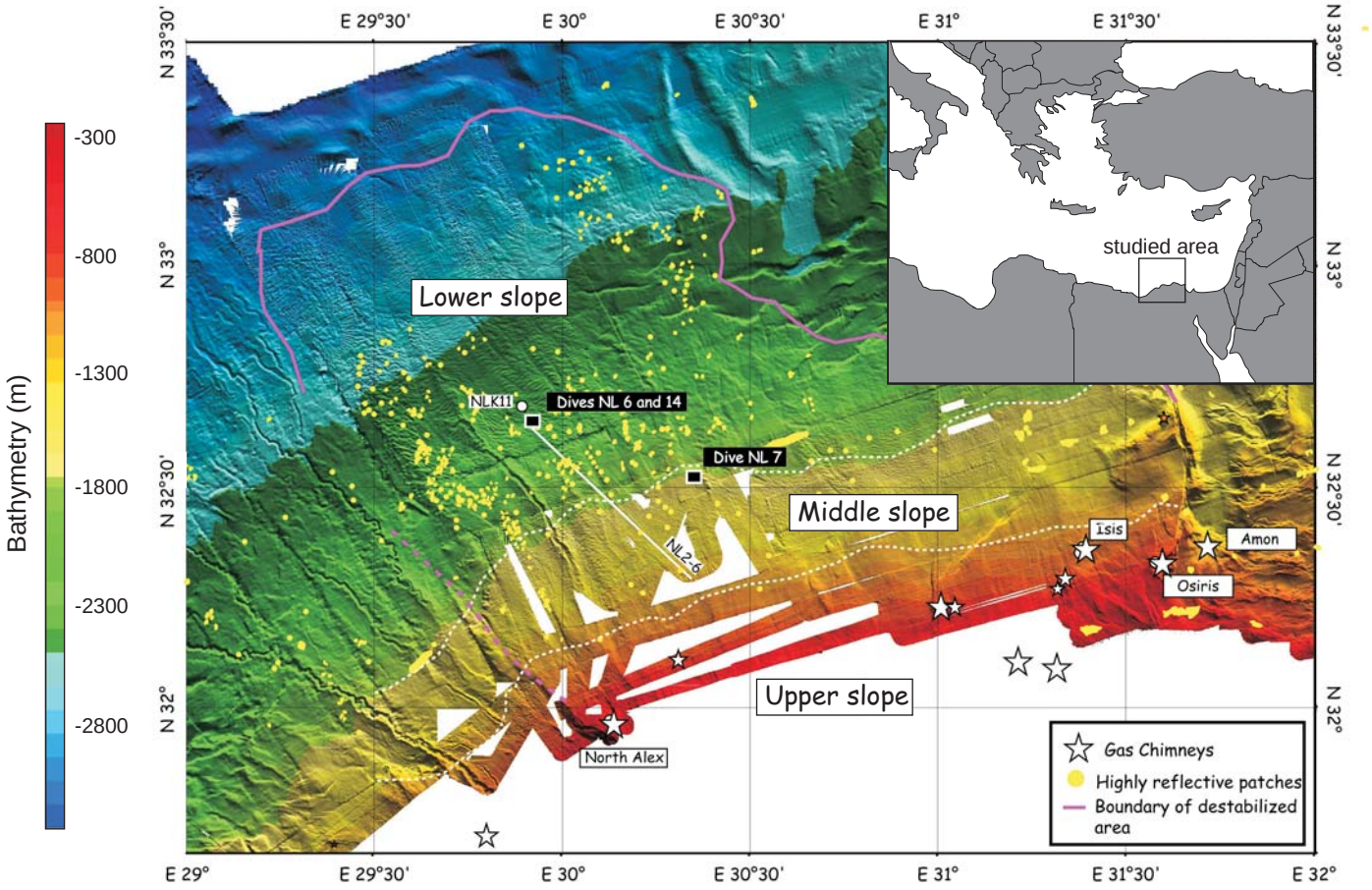
Bathymetry (m)
-300
-800
-1300
-1800
-2300
-2800
E 29°
E 29°30'
E 30°
E 30°30'
E 31°
E 31°30'
E 32°
N 33°30'
N 33°
N 32°30'
N 32°
studied area
Lower slope
Middle slope
Upper slope
NLK11
Dives NL 6 and 14
Dive NL 7
NL2-6
Isis
Amon
Osiris
North Alex
Gas Chimneys
Highly reflective patches
Boundary of destabilized area

Fig1

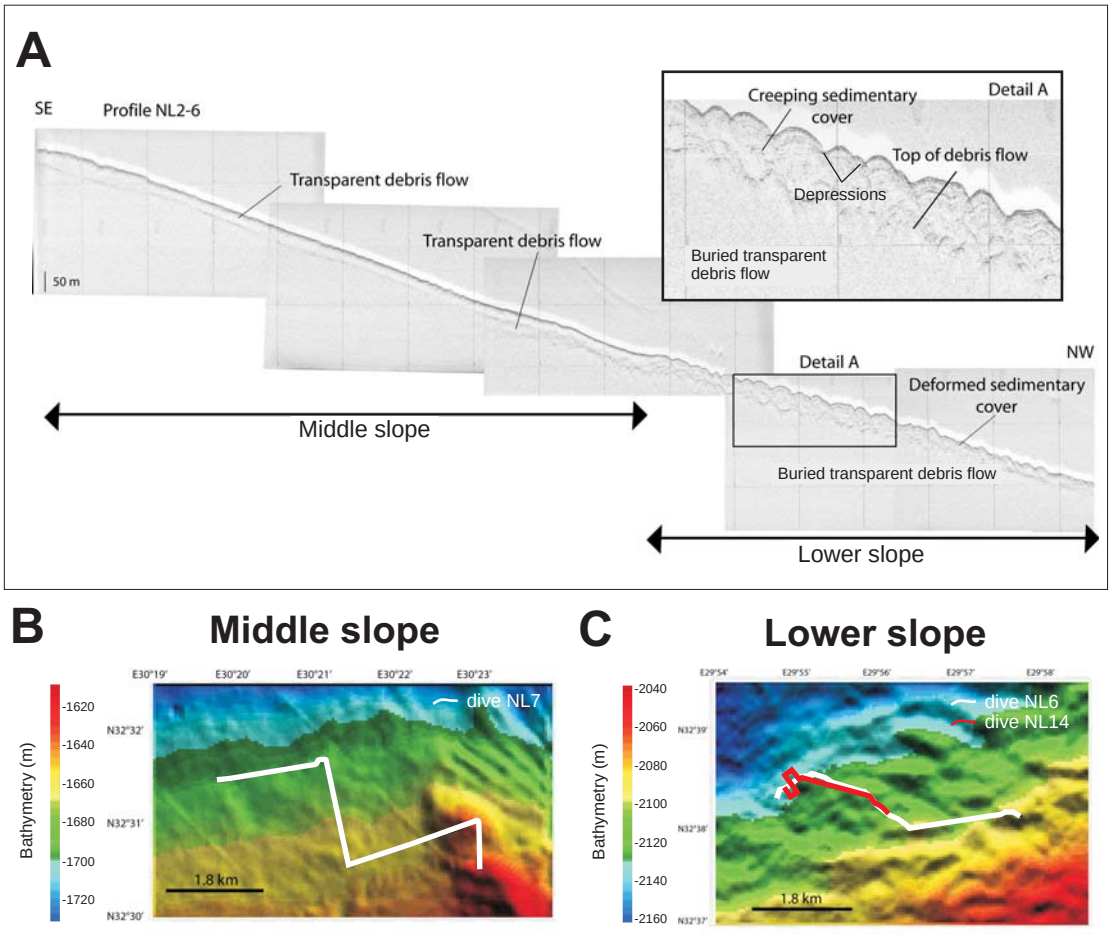
A
SE
Profile NL2-6
Transparent debris flow
Transparent debris flow
50 m
Middle slope
Creeping sedimentary cover
Detail A
Top of debris flow
Depressions
Buried transparent debris flow
Detail A
NW
Deformed sedimentary cover
Buried transparent debris flow
Lower slope
B
Middle slope
Bathymetry (m)
-1620
-1640
-1660
-1680
-1700
-1720
E30°19'
E30°20'
E30°21'
E30°22'
E30°23'
N32°32'
N32°31'
N32°30'
dive NL7
1.8 km
C
Lower slope
Bathymetry (m)
-2040
-2060
-2080
-2100
-2120
-2140
-2160
E29°54'
E29°55'
E29°56'
E29°57'
E29°58'
dive NL6
dive NL14
1.8 km

Fig2

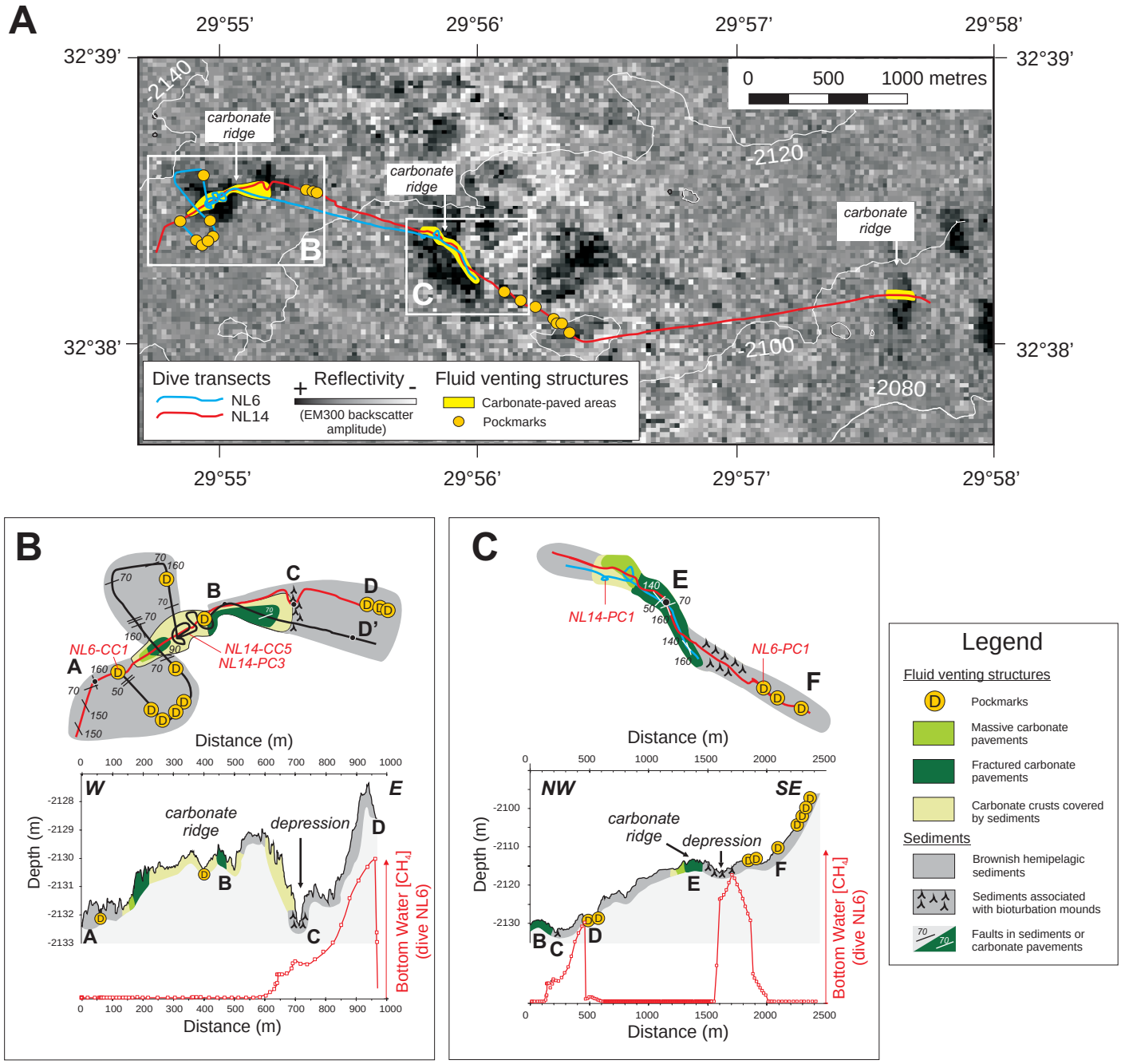
A
29°55'
29°56'
29°57'
29°58'
32°39'
32°38'
0 500 1000 metres
-2140
-2120
-2100
-2080
carbonate ridge
carbonate ridge
carbonate ridge
B
C
Dive transects
NL6
NL14
Reflectivity
(EM300 backscatter amplitude)
Fluid venting structures
Carbonate-paved areas
Pockmarks
B
NL6-CC1
NL14-CC5
NL14-PC3
Distance (m)
W
E
carbonate ridge
depression
Depth (m)
Bottom Water [CH4] (dive NL6)
C
NL14-PC1
NL6-PC1
NW
SE
Legend
Fluid venting structures
Pockmarks
Massive carbonate pavements
Fractured carbonate pavements
Carbonate crusts covered by sediments
Sediments
Brownish hemipelagic sediments
Sediments associated with bioturbation mounds
Faults in sediments or carbonate pavements

Fig3

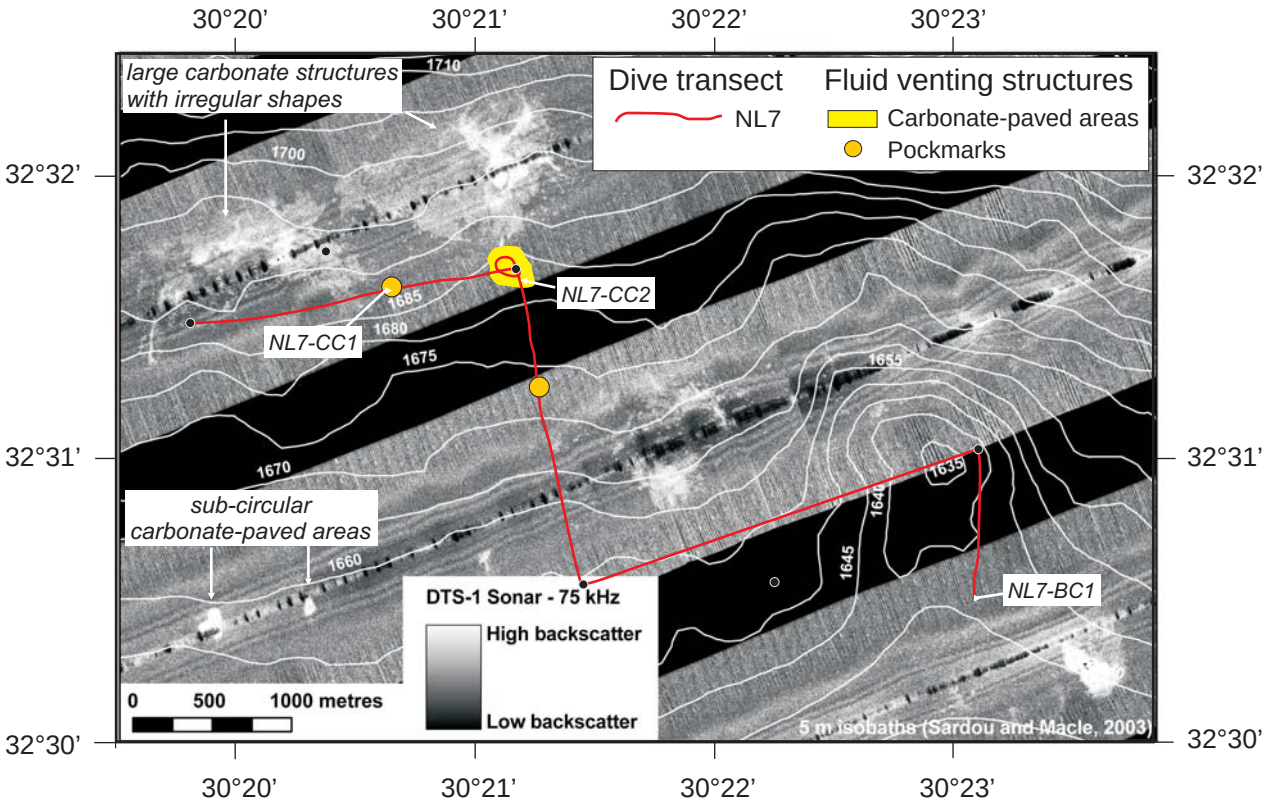
30°20'
30°21'
30°22'
30°23'
32°32'
32°31'
32°30'
large carbonate structures with irregular shapes
Dive transect
NL7
Fluid venting structures
Carbonate-paved areas
Pockmarks
NL7-CC2
NL7-CC1
NL7-BC1
sub-circular carbonate-paved areas
DTS-1 Sonar - 75 kHz
High backscatter
Low backscatter
0 500 1000 metres
5 m isobaths (Sardou and Macle, 2003)
1710
1700
1685
1680
1675
1670
1660
1655
1645
1635

Fig4

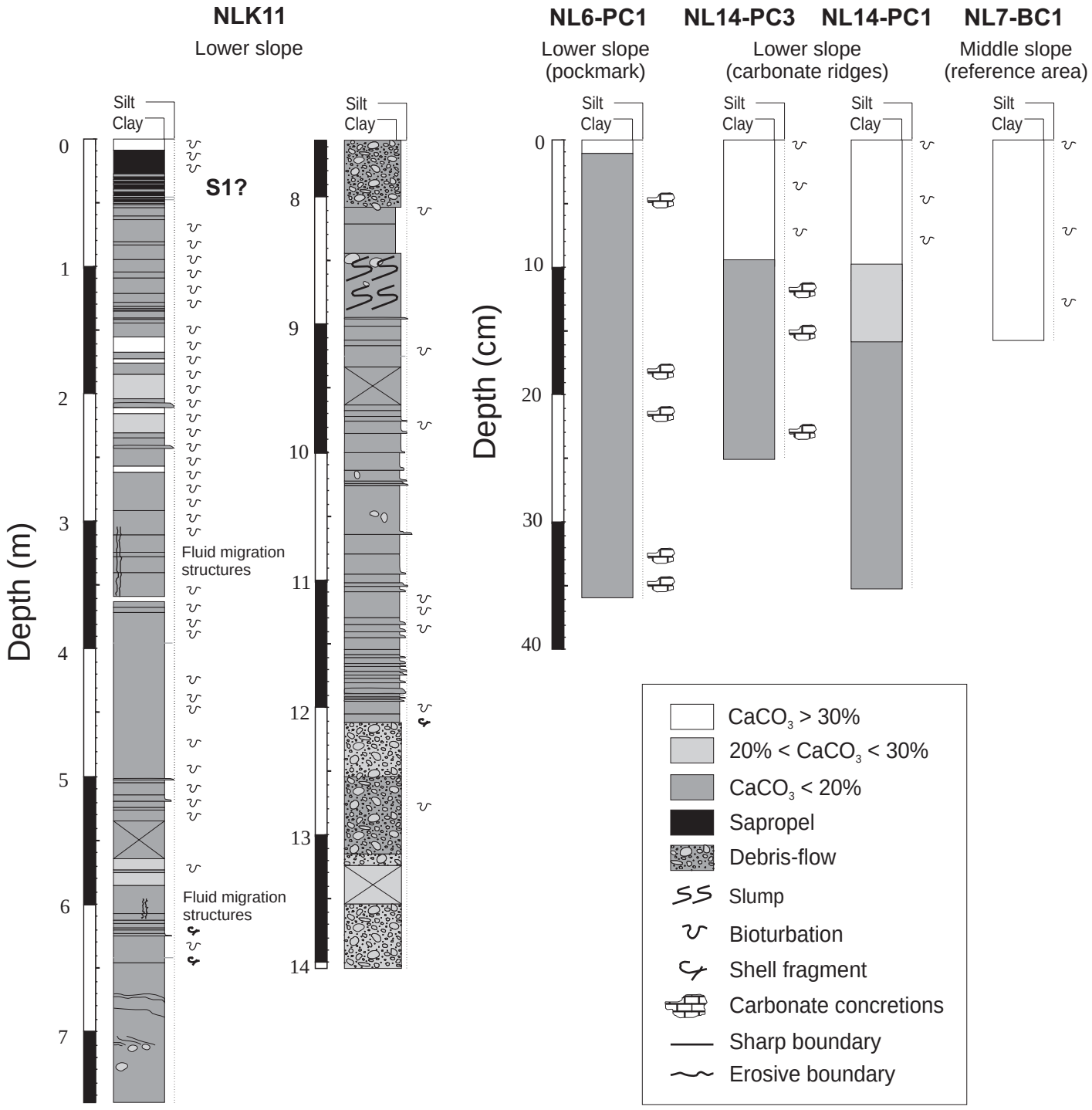
NLK11
Lower slope
Silt
Clay
S1?
Depth (m)
Fluid migration structures
Fluid migration structures
NL6-PC1
Lower slope (pockmark)
NL14-PC3
NL14-PC1
Lower slope (carbonate ridges)
NL7-BC1
Middle slope (reference area)
Depth (cm)
CaCO3 > 30%
20% < CaCO3 < 30%
CaCO3 < 20%
Sapropel
Debris-flow
Slump
Bioturbation
Shell fragment
Carbonate concretions
Sharp boundary
Erosive boundary

Fig5

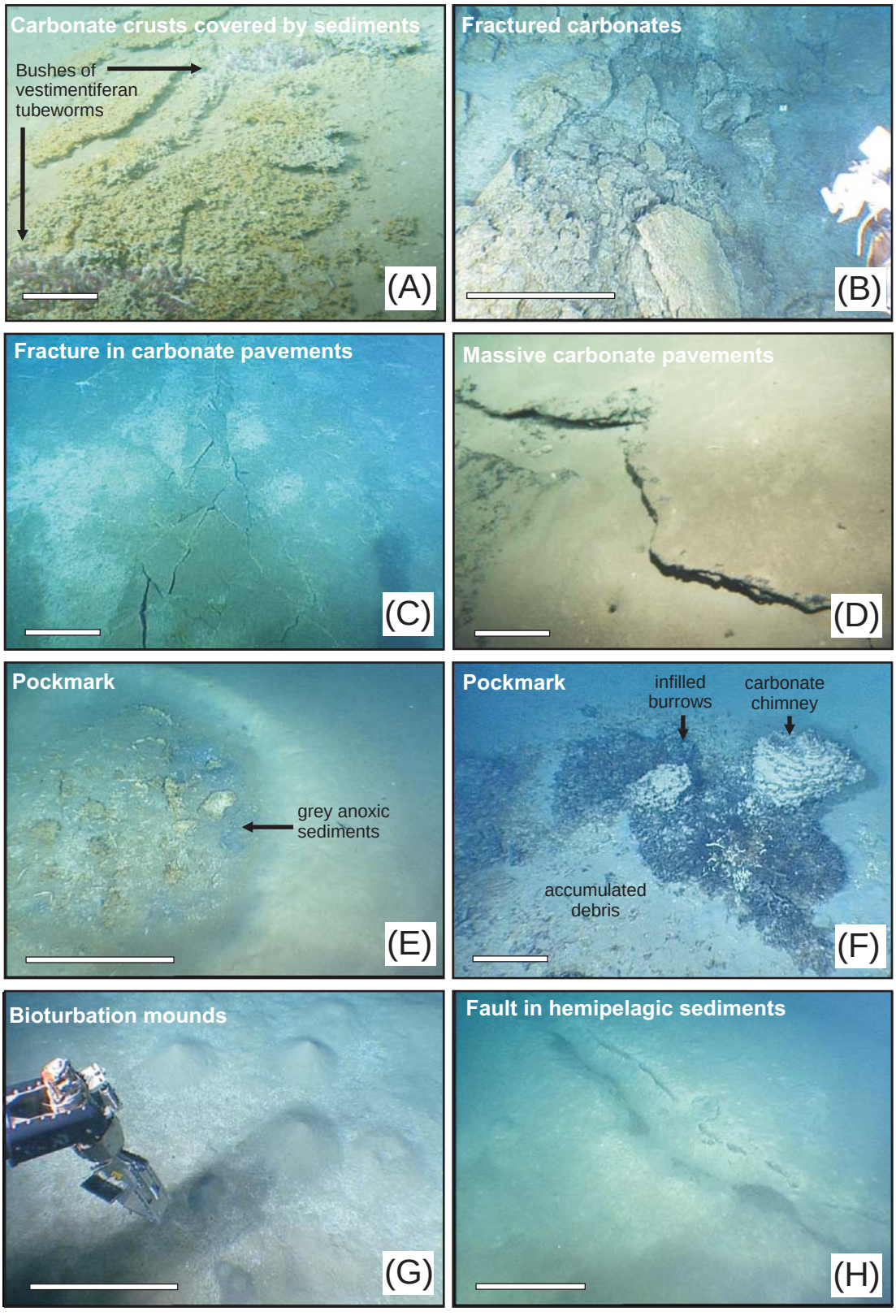
Carbonate crusts covered by sediments
Bushes of vestimentiferan tubeworms
(A)
Fractured carbonates
(B)
Fracture in carbonate pavements
(C)
Massive carbonate pavements
(D)
Pockmark
grey anoxic sediments
(E)
Pockmark
infilled burrows
carbonate chimney
accumulated debris
(F)
Bioturbation mounds
(G)
Fault in hemipelagic sediments
(H)

Fig6

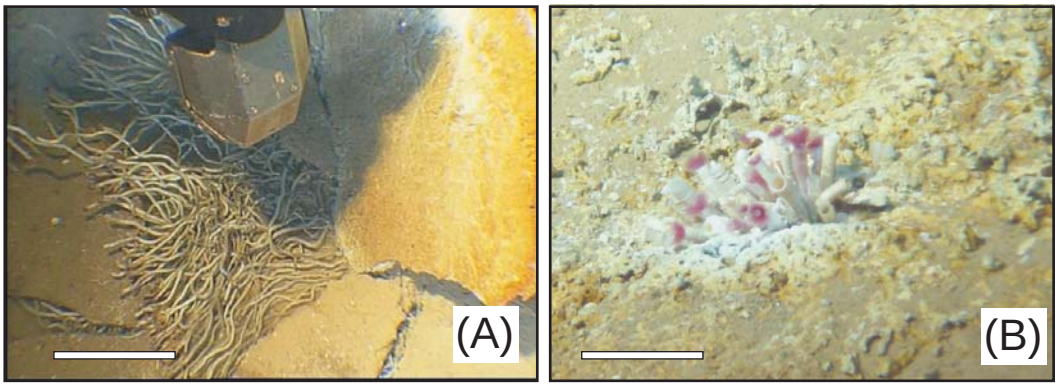

Fig7

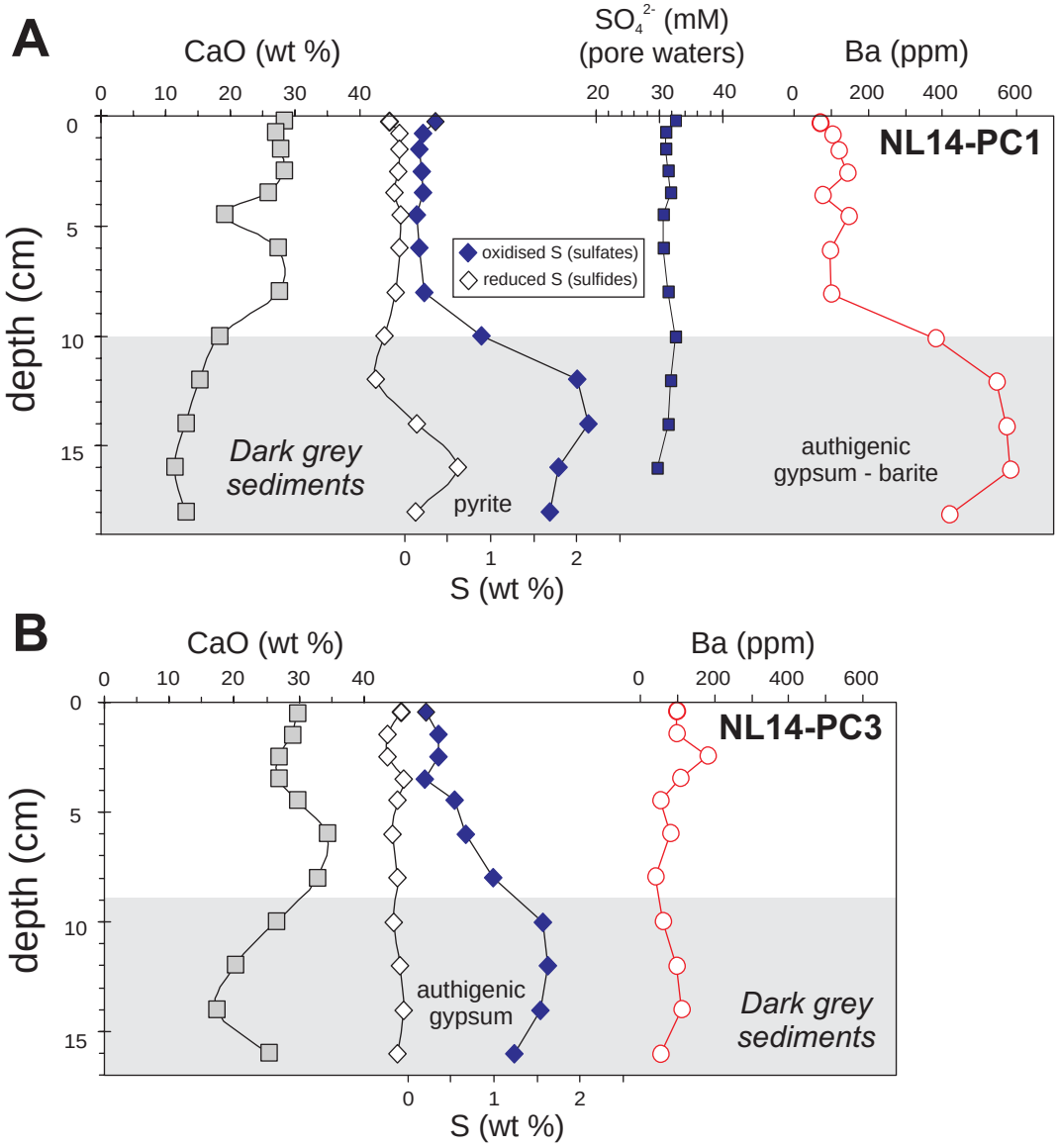
A
CaO (wt %)
SO_4^{2-} (mM)
(pore waters)
Ba (ppm)
NL14-PC1
depth (cm)
oxidised S (sulfates)
reduced S (sulfides)
Dark grey
sediments
pyrite
authigenic
gypsum - barite
S (wt %)
B
CaO (wt %)
Ba (ppm)
NL14-PC3
depth (cm)
authigenic
gypsum
Dark grey
sediments
S (wt %)

Fig8

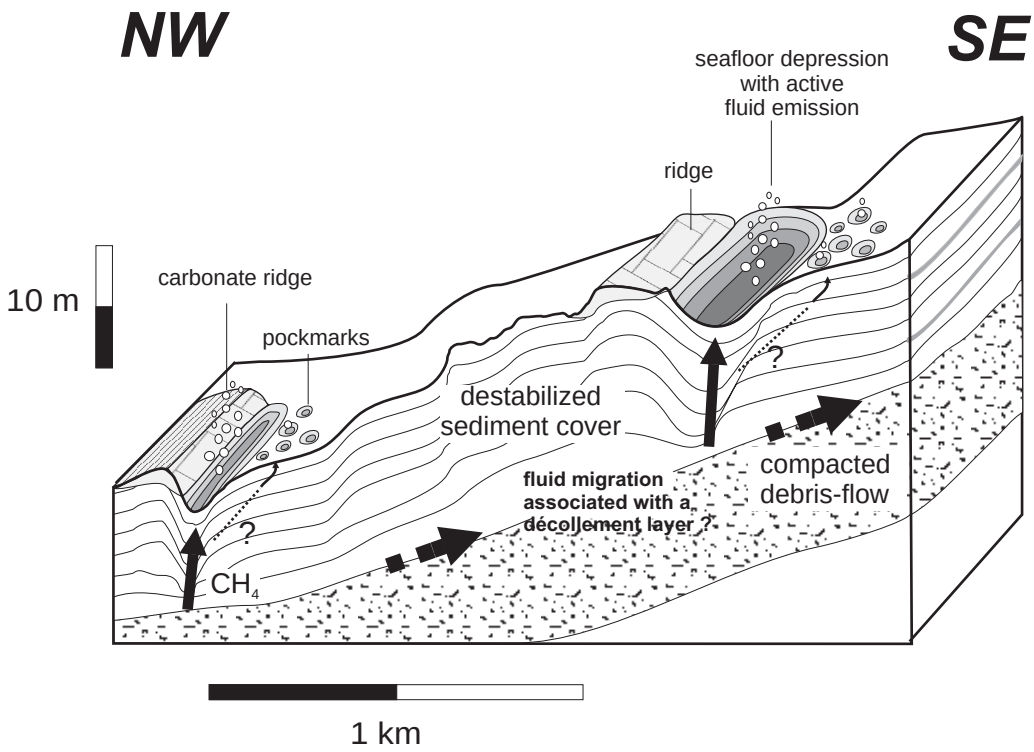
NW
SE
seafloor depression
with active
fluid emission
ridge
10 m
carbonate ridge
pockmarks
destabilized
sediment cover
compacted
debris-flow
fluid migration
associated with a
décollement layer ?
CH4
?
?
1 km

Fig9